# Photoinduced charge separation in functional carbon-silver nanohybrids

M. Reale[a], S. Chandra[b], G. Buscarino[a,c], A. Emanuele[a], M. Cannas[a], O. Ikkala[b], A. Sciortino[*a,c], F. Messina[**a,c]

[a] Dipartimento di Fisica e Chimica – Emilio Segrè, Università degli Studi di Palermo, Via Archirafi 36, 90123 Palermo (Italy)
[b] Department of Applied Physics, Aalto University, P. O. Box 15100, Espoo, FI-00076, Finland
[c] ATeN Center – Università degli Studi di Palermo, Viale delle Scienze, Edificio 18, 90128 Palermo (Italy)

[*] alice.sciortino02@unipa.it
[**] fabrizio.messina@unipa.it

## Abstract

In recent times, nanoscience is devoting a growing interest in the easy assembly of well-established nanomaterials into hybrid nanostructures displaying new emerging features. Here, we study the photo-physicochemical response of binary nanohybrids obtained through the spontaneous coupling of luminescent carbon dots to silver nanoparticles with controlled surface charge. Evidence of the successful couplings is obtained by steady-state and time resolved optical measurements, and further confirmed by direct imaging. We demonstrate strong interactions within the nanohybrids, which can be modelled in terms of a sub-picosecond electron-transfer from photoexcited carbon dots to silver nanoparticles. Accordingly, the newly designed nanohybrids display a significant photocatalytic performance demonstrated by the photodegradation of methylene blue under ultraviolet-visible light. Our results provide an exhaustive picture of the optical response of these self-assembled carbon-silver nanohybrids, and show their promise as a new class of eco-friendly materials for light-driven catalytic applications.

# Introduction

Carbon dots (CDs) are a relatively novel family of quasi-spherical nanoparticles with a size < 10 nm, constituted by a carbonaceous core decorated by a surface shell rich of nitrogen- and oxygen-containing functional groups. Since their accidental discovery [1], an extensive and interdisciplinary research has been conducted on their fascinating fluorescent properties, which make CDs one of the most appealing luminescent nanomaterials emerging in the last decade. The bright and tunable fluorescence of CDs is accompanied by high photo/thermostability, water solubility and biocompatibility [2], as well as low cost and ease of synthesis procedures [3, 4]. The combination of these characteristics leads to several optoelectronics [5, 6], sensing [7, 8] and biomedical applications [9, 10], making CDs extremely promising as a potential alternative to the more common organic dyes or semiconductive quantum dots, the use of which is often limited by higher toxicity and cost.

Nowadays, a great attention is being devoted in material science to the design of nanohybrids [11, 12] that exploit the combination of different nanomaterials to obtain specific functional features generally absent in the individual components, as for example photocatalytic or photovoltaic properties. Due to the abundance and chemical versatility of their surface functional groups, CDs possess particularly beneficial characteristics to be incorporated in more complex structures by coupling them to other species [13] such as polyoxometalates [14], porphyrins, carbon nanotubes [15], polymers [16]. Interestingly, the strong UV-VIS light absorption and electron-transfer features of CDs are very appealing to carry out solar-driven catalytic processes, either by acting directly as photocatalysts [17, 18, 19] or by forming composite catalysts with other suitable nanomaterials [20, 21]. For example, several works have studied the nanosystems obtained by adsorbing CDs on semiconductor surfaces, demonstrating their use to harvest solar energy in dye-sensitized solar cells [22], or to improve the visible-light photocatalytic performances of semiconductive nano-oxides (e.g. $TiO_2$, ZnO [23, 24] and $Cu_2O$ [25]).

In contrast, very few studies have investigated the coupling of CDs to metallic nanoparticles (MNPs), such as nano-silver or gold (AgNPs and AuNPs, respectively). Indeed, the attachment of CDs to metallic nanoparticles should favor the constitution of photo-excitable states with a strong degree of charge separation, enhanced by the high carrier mobility in the metallic component. The sparse literature on the subject has hitherto been limited only to disclose the effect of plasmonic nanoparticles on the steady-state photoluminescence properties of CDs [26, 27, 28], scarcely investigating the potential enhancement of photocatalytic properties. Furthermore, the photophysical behavior of CD-MNP composites has not been studied in detail.

Here we report binary CD@AgNP hybrids obtained via an easy and inexpensive self-assembly strategy founded on the spontaneous electrostatic coupling of CDs and AgNPs with controlled surface charges. We show that these CD@AgNPs nanohybrids exhibit photocatalytic activity which is absent in CDs or AgNPs taken individually. This emerging property is due to the ease of CDs to undergo photoinduced charge transfer [29], acting in synergy with the high carrier mobility within AgNPs. In this respect, we provide experimental evidence of very fast photoinduced electron-transfer from CDs to AgNPs (< 300 femtoseconds) followed by a much slower back-electron-transfer which ultimately cuts off the photocycle of the nanohybrid. Our results pave the way to a new generation of nanoscale hybrids with notable charge separation and light-driven catalytic properties, and contribute to clarify the interaction pathways between CDs and metal nanoparticles.

# Experimental Section

**Samples preparation**

CDs were synthesized by the microwave-induced hydrothermal decomposition of an aqueous solution of citric acid and urea, in a 1:1 weight ratio. This procedure permits to obtain CDs of 3-8 nm diameter characterized by a carbon nitride core structure and a functionalized surface rich of polar groups. For a full description, we refer to the characterization already reported in our previous works [30,31]. In particular, the knowledge of their molar extinction coefficient permitted to estimate molar concentration of CD nanoparticles directly from optical absorption measurements.

The plasmonic silver nanoparticles AgNPs were obtained by a synthetic route inspired by the well-known Turkevich method, one of the milestones of metallic nanoparticles synthesis [32]. Briefly, 50 mL of 5 mM citric acid solution was adjusted to pH 7 by adding about 20 mL of a NaOH solution, and then it was heated under vigorous stirring. Once reached the boiling point, 1 mL volume of 25 mM $AgNO_3$ solution was quickly added to the initially colourless solution which, after about ten minutes, began to acquire a yellowish hue. The heating was stopped after 30 minutes, when the solution had turned a brownish-yellow colour resulting quite turbid, after which it was naturally cooled at room temperature. Subsequently, in order to remove residual reagents, the mixture was subjected to two cycles of centrifugation (8000 rpm for 15 minutes) and subsequent redispersion of sediment in milli-Q water, after decantation of the supernatant. The molar concentration of silver nanoparticles was calculated from the maximum absorbance at the UV-Vis spectra [33], having estimated their size by atomic force microscopy and transmission electron microscopy.

In the just described route the sodium citrate ions play the role of both reducing and capping agent, such that the AgNPs are characterized by a negatively charged surface shell. For this reason, we denote them as AgNP-. Starting from these, a second family of silver nanoparticles AgNP+ with opposite surface charge was also obtained via a ligand exchange procedure: 2 mL of AgNP- solution were added dropwise into 2 mL of a 2 mM cetyltrimethylammonium bromide (CTAB) solution and the mixture was gently stirred for 24 hours. Both the colloidal solutions of AgNP- and AgNP+ are stable for several weeks when stored at 4°C and show no signs of aggregation, as confirmed by their extinction spectra and repeated dynamic light scattering (DLS) measurements.

**Atomic Force Microscopy (AFM)**

In order to perform AFM studies, a drop of aqueous solution of the sample was deposited on a mica substrate and left to dry under vacuum. AFM images were obtained by using a Bruker FAST-SCAN microscope, equipped with a closed-loop piezoscanner (maximum x-y range about 34 um and maximum z range about 3 um) and a four-segment photodetector for cantilever deflection monitoring. The scans were carried out in soft tapping mode by using a FASTSCAN-A probe with a tip radius of about 5 nm and setting a pixel resolution comparable to this tip size. The diameter of the nanoparticles was estimated by evaluating their height.

**Dynamic Light Scattering (DLS)**

DLS correlation functions were measured on samples, highly diluted to limit scattered intensity, by using a Brookhaven BI-200SM goniometer equipped with Perkin-Elmer Optoelectronics APD (SPCM-AQR-14) and a Flex-01 1088 channel multitau correlator. A 671 nm laser light was used.

**Zeta potential**

Zeta-potential measurements were acquired on 1 mL of aqueous sample using a Malvern Zetasizer NanoZS instruments equipped with a 632 nm laser with a fixed scattering angle of 173°, and Dispersion Technology Software 7.02 software (Malvern Panalytical ltd, Almelo, The Netherlands). The zeta-potential values (mV) were obtained from electrophoretic mobility by means of the Smoluchowski equation. All analyses were performed in triplicate.

**High-resolution transmission electron microscopy (HRTEM)**

HR-TEM images were captured using JEM-2200FS Double Cs-corrected transmission electron microscope. The instrument was operated at an acceleration voltage of 200 kV with field-emission guns. Specimens for HR-TEM analyses were prepared by drop-casting from the aqueous dispersion

of the sample in ultrathin-carbon (<10 nm thickness) coated copper grids. The sample were drop casted onto a copper TEM grid with carbon film (CF200-Cu-UL, Electron Microscopy Sciences) and incubated for 5 mins, after which the excess materials were washed with water and finally dried in air.

**Attenuated Total Reflection (ATR) Infrared Spectroscopy**

ATR measurements were performed by means of a Platinum ATR spectrometer (Bruker, Billerica) equipped with a single-reflection diamond crystal. ATR spectra in the 500-3500 $cm^{-1}$ spectral region were acquired by depositing a drop of concentrated CD aqueous solution on the sample holder of the instrument and letting the solvent dry out. In order to increase the signal-to-noise ratio, several measurements were repeated and averaged.

**Steady-State Spectroscopy**

The absorption spectra were acquired on aqueous solutions in a 1 cm cuvette by using a single-beam optical fiber spectrophotometer (Avantes) using a dual halogen-xenon light source ensuring the investigation of a spectral window between 250 and 800 nm. The photoluminescence spectra were recorded on aqueous solutions in a 1 cm cuvette with a JASCO FP6500 spectrofluorometer with a 3 nm bandwidth, equipped with a 150 W Xenon lamp as excitation source and a photomultiplier as detection system, operating in the range of 400-700 nm.

**Time-resolved Fluorescence Spectroscopy**

Time-resolved photoluminescence measurements were carried out by the use of a tunable laser system consisting in an optical parametric oscillator pumped by the third harmonic of a Q-switched Nd:YAG laser providing 5 ns pulses at 10 Hz repetition rate. The dispersed emission spectrum of the sample, located in a 1 cm cuvette, is thus recorded on an intensified CCD camera (with a spectral resolution of 3 nm), at a certain delay from the laser pulse and for a chosen time window of 1 ns. Therefore, the acquisition of the emission at different delays from the excitation permits to get the time-resolved spectral evolution of the sample, with a time resolution of 0.2 ns.

**Femtosecond-resolved transient absorption**

Transient absorption (TA) experiments were performed by the use of a Ti:Sapphire ultrafast amplifier laser (Solstice-Ace) generating 45 fs pulses peaked at 800 nm. The beam is split in two (80%/20%) in order to generate the pump and probe pulses. The former is obtained by frequency doubling the 800 nm beam in a 250 μm thick BBO which allows to obtain 400 nm pulses. The latter

is a supercontinuum pulse covering the 400-700 nm spectral range, obtaining by focusing the 800 nm beam in a 2 mm quartz cuvette containing $D_2O$. Pump-probe delay is controlled by a motorized delay stage. The pump is chopped at 2500 Hz in order to alternatively record the pump and unpumped spectra. Both beams are focused and overlapped on the sample which continuously flows in a 0.2 mm flow cell. After passing through the sample, the probe is dispersed by means of a Brewster-angle silica prism and focused by a lens on a single shot detector (Glaz-LineScan-I). The used configuration guarantees a spectral resolution of 3 nm and a temporal resolution of 150 fs. All the TA measurements were made in linear regime with an energy of about 50 nJ per pulse, under the so-called magic angle detection conditions. The TA data here reported were subjected to standard correction procedures to eliminate the effects of cross phase modulation (XPM) and group velocity dispersion (GVD) [34].

**Photocatalysis setup**

Photocatalysis experiments were carried out by illuminating samples by a 50 W Xenon lamp, whose light was directed through an optical fiber to irradiate the solutions placed inside a glass cuvette (1 cm). The photocatalysis experiments were set up in order to permit the real-time acquisition of the sample absorbance spectrum *in situ* during illumination. To this purpose, we used the same light source also as probing light, attenuated by means of neutral density filters positioned after the sample, and then collected on the optical fiber spectrophotometer. In each photocatalysis experiment a 5 % v/v of 2-propanol was added to the solution, to play the role of hole scavenger.

# Results and Discussion

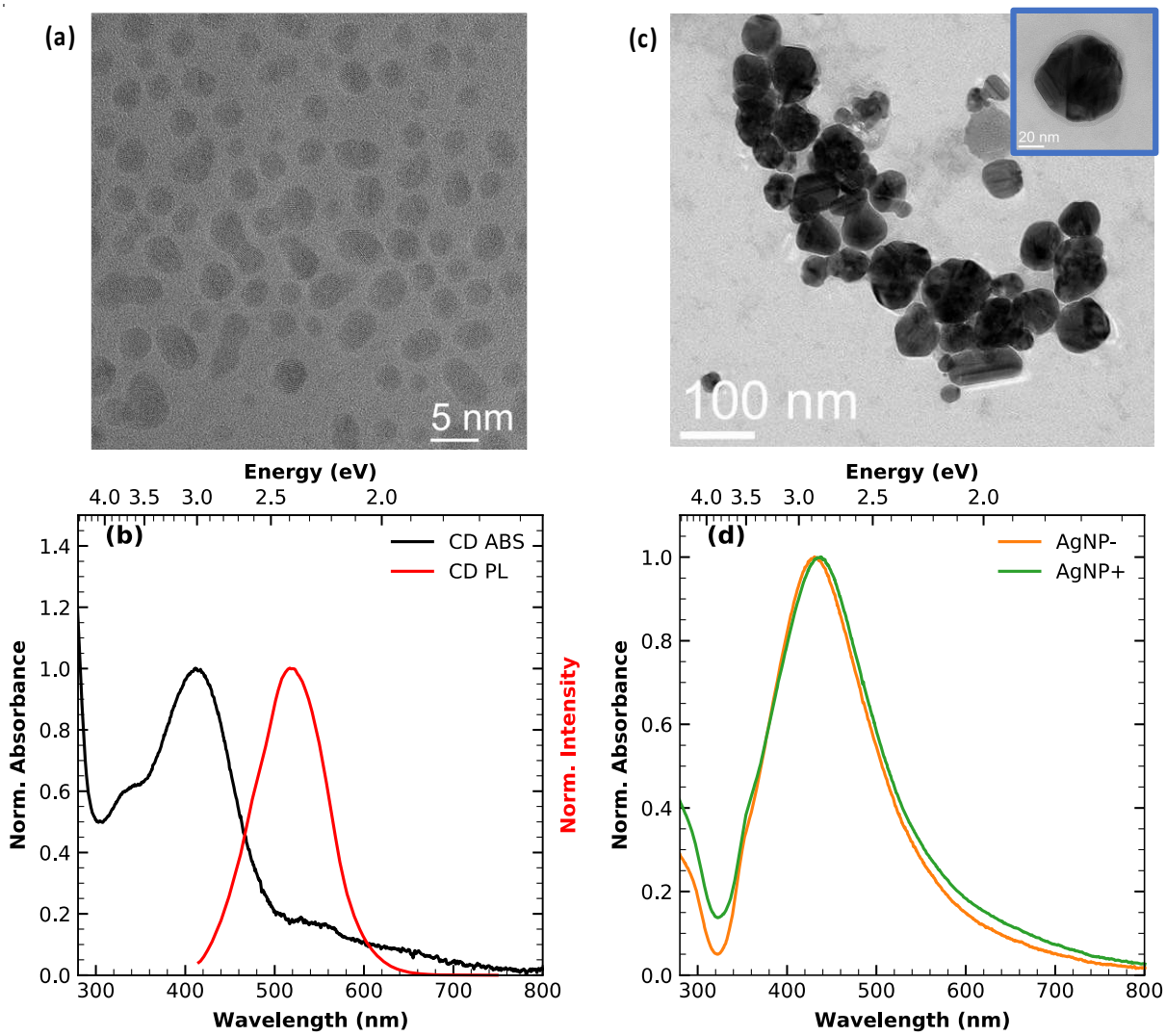


*Figure 1 – (a) HRTEM image of CDs. (b) Steady-state optical properties of CDs in water: normalized UV-VIS absorption spectrum (black) and photoluminescence spectrum upon 400 nm excitation (red). (c) TEM image of as-synthetized citrate-capped AgNP-. The capping layer is well visible in the HRTEM image reported in the upper right sub-panel. (d) Comparison of normalized extinction spectra of AgNP- (orange) and CTAB-capped AgNP+ (green) obtained via ligand exchange.*

Figure 1 provides an overview of the main structural and optical properties of the bare CDs and silver nanoparticles. The nitrogen-doped CDs used in this work are obtained through a simple bottom-up approach involving a thermally-induced decomposition method, as reported in our previous works [31]. As visible from Fig. 1a, these CDs display well-defined carbonaceous cores with average sizes of about 3 nm and a good degree of crystallinity. Infrared absorption studies (Figure S1) show that

their disordered surface shell mostly consists in carboxylic and hydroxyl moieties. Dissociation of carboxylic surface groups imparts a negative net surface charge in water, as revealed by the measured zeta potential value of -15±5 mV at a neutral pH value. In Figure 1(b), the black curve represents the UV-VIS absorption spectrum of CDs dispersed in water. While the absorption edge at wavelengths below 300 nm is ascribable to band-to-band core transitions, the strong and peculiar absorption band peaking at 410 nm is typical of nitrogen-rich bottom-up CDs [35, 36] and it is due to a sub-gap transition involving the migration of an electron from the inner core of CDs to surface charge traps [37]. Excitation within the 410 nm absorption band gives rise to an unstructured emission peaking around 525 nm (solid red curve), characterized by an emission quantum yield of 12±1%.

The silver nanoparticles we aimed to couple to the CDs, were synthesized through a synthetic route based on the well-known Turkevich method [32], fully described in the experimental section. A transmission electron microscopy image of the so-synthesized citrate-capped silver nanoparticles is reported in Figure 1(c). It shows that most nanoparticles have a quasi-spherical shape, with a broad distribution of sizes. Together with the spherical-shaped AgNPs, a few nanorods are observed, whose anisotropic morphology could make the optical absorption dependent on polarization [38]. However, such an effect is not observable here, being the nanohybrids randomly oriented in solution. The particle sizes were also assessed through atomic force microscopy (AFM) and dynamic light scattering (DLS) measurements, from which we obtained specifically a mean effective diameter of $50 \pm 20$ nm by AFM (Figure S2) and a mean hydrodynamic diameter of $52 \pm 6$ nm by DLS (Figure S3).

In general, the properties of composite nanohybrids could significantly depend on every specific physicochemical characteristic of the precursor materials, such as size, shape and surface charge [39]. Here in particular, the sign and magnitude of AgNP surface charge is expected to be critical in determining the ease of coupling to CDs. Therefore, in order to produce two typologies of identical AgNPs only differing for the surface charge sign, we applied on the as-synthesized citrate-capped AgNP- a ligand-exchange procedure by positively-charged cetyltrimethylammonium bromide (CTAB) molecules to obtain positively surface charged AgNP+. The ligand-exchange reaction is inspired by previous works [40, 41] and described in detail in the experimental section. Success of the ligand exchange was confirmed by the two surface charges of opposite sign obtained by zeta potential measurements, specifically $\zeta = -23 \pm 5$ mV for the citrate-capped AgNP-, readily obtained by the synthetic route, and $\zeta = +33 \pm 6$ mV for the CTAB-capped AgNP+ after ligand exchange. The different surface capping also leads to a small, but appreciable, shift between the plasmonic bands characterizing the optical extinction spectra overlayed in Figure 1(d): $\lambda_{peak} =$

431 ± 1 nm for AgNP-, while $\lambda_{peak} = 437 \pm 1$ nm for AgNP+. This shift is indeed compatible with the different environment experienced by the two types of AgNPs [42].

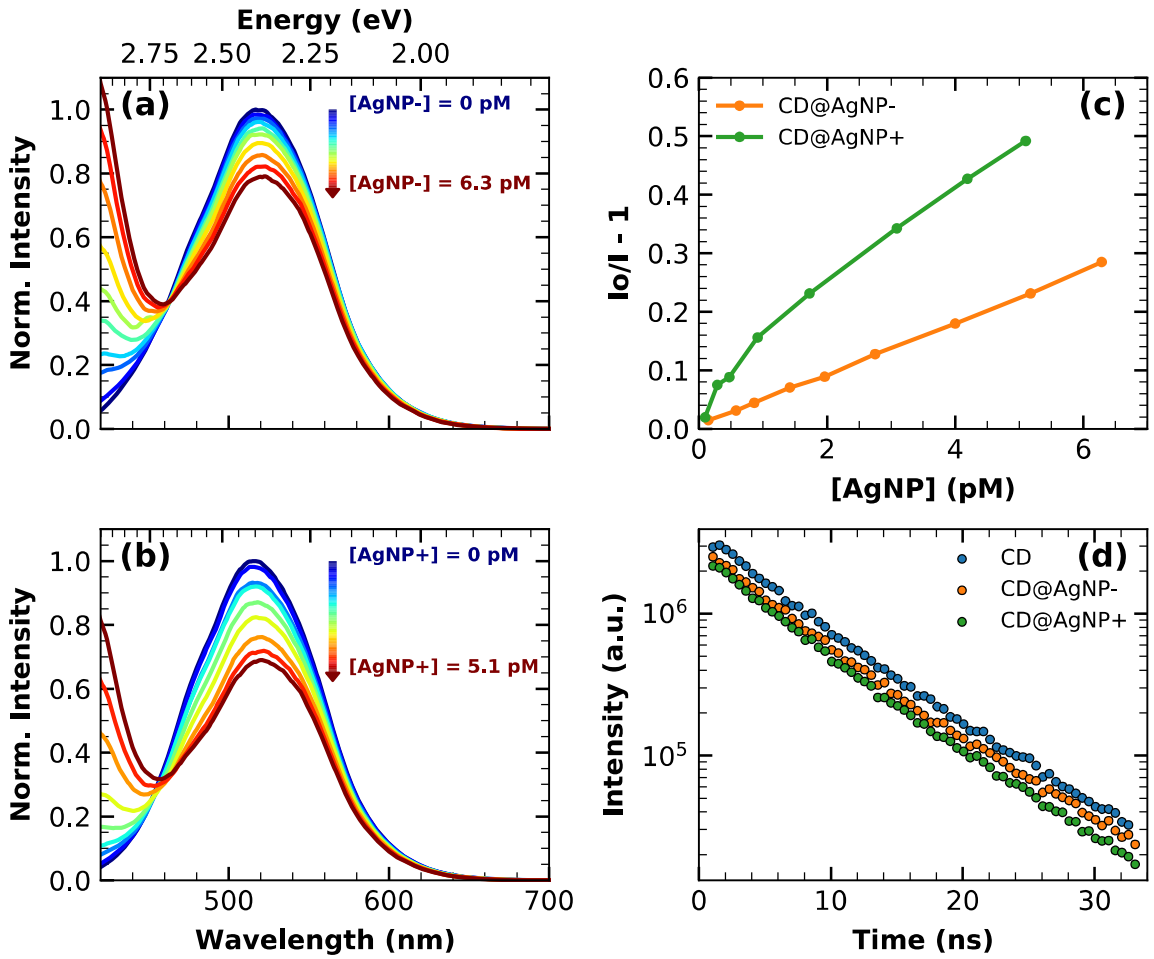


*Figure 2 – Photoluminescence spectra under 410 nm excitation of the CD solution (60 nM) in the presence of increasing amount of (a) AgNP- and (b) AgNP+ as indicated by the arrows. (c) Stern-Volmer plots of CDs emission intensity quenched by AgNP- (orange) and AgNP+ (green). (d) Emission decay traces collected from solutions of pure CDs 60 nM (blue), of CDs 60 nM with addition of 6 pM AgNP- (orange) and of CDs 60 nM with addition of 5 pM AgNP+ (green).*

Optical measurements were used to probe the possible interactions between CDs and AgNPs, so as to obtain clues about the formation of complexes of the two species in solution. To this purpose, variable, small aliquots of a concentrated AgNP solution were added to 2 mL of an aqueous dispersion of CD nanoparticles at 60 nM concentration, in order to allow CDs to interact with increasing concentrations of AgNPs (calculated, for each addition, by taking into account their dilution into the CD solution). Then, photoluminescence spectroscopy was used to monitor the interactions between the two nanoobjects. Figures 2a and 2b show the photoluminescence spectra of CDs acquired at an

excitation wavelength of 410 nm as a function of molar concentrations of AgNP- and AgNP+ nanoparticles concentrations, respectively. The emission spectra in Figure 2 were also corrected for the dilution induced by the addition of AgNP solutions, and for the inner filter effect of the silver nanoparticles on the excitation beam. In contrast, reabsorption of CD emission from AgNPs can be shown to be negligible in the concentration range reported in Figure 2. In fact, the comparisons in Figure S4(a) and S4(b), where the normalized emission spectra of Figure 2a and 2b are shown respectively, display no significant changes of the emission band-shape, confirming the absence of reabsorption effects, which otherwise would have caused a distortion of the CD photoluminescence (PL) band, due to its partial overlap with the absorbance band of AgNPs. In fact, higher concentration of AgNPs would have increased the optical density of the solution, causing much more marked inner filter effects which could be misinterpreted as a pure quenching.

From Figure 2, we can conclude that CD emission undergoes a continuous quenching upon addition of both types of AgNPs, suggesting that simply by adding AgNPs to a solution of CDs, some kind of interaction is quickly established between the two. Indeed, a small but appreciable quenching of the emission band is registered already at the first addition of AgNPs despite their extremely low concentration (< 1 pM). Beside quenching, the increase of AgNPs concentration determines an enhancement of the excitation light scattered on the detector, as evident from the increase of the excitation peak in Figure 2(a) and (b).

The Stern-Volmer graphs of Figure 2(c), where the quantity $I_0/I - 1$ is reported *vs* AgNPs concentration, provide a quantitative picture of the quenching phenomenon. The clear linear trend encountered for CD@AgNP- is not found for CD@AgNP+, which shows a markedly higher slope at low AgNP+ concentrations (< 1 pM), that decreases afterwards. Most importantly, the quenching generated by the positive nanoparticles is two to four times greater with respect to the negative particles. This result is consistent with the oppositely-charged nature of the surfaces of AgNP+ and CDs, which is expected to favor their coupling into a nanohybrid. However, the existence of a PL quenching also with AgNP-, albeit to a lower extent, suggests that the interaction between the two precursors is not purely electrostatic. In CD@AgNP+ nanohybrids, the positively charged quaternary amine on the CTAB layer covering the AgNPs should strongly interact with negatively charged $COO^-$ groups on CD surfaces. Yet, the nonlinear trend of the Stern-Volmer plot suggests at least two geometrical configurations characterized by different CD-AgNP binding constants. In contrast, the formation of CD@AgNP- nanohybrids is most likely mediated by hydrogen bonding interactions between citrate ions on AgNPs and either -OH or -COOH groups on CDs. Further studies are needed to address in more details the bonding pathways within CD@AgNP nanohybrids. In the rest of this study, we will mostly focus on their photophysical behaviour and photocatalytical function.

Further evidence of the successful CDs-AgNPs coupling is provided by the modifications encountered in the absorbance spectra. In fact, the extinction spectra of CD@AgNP nanohybrids does not trivially correspond to the sum of the spectra of the two individual starting constituents, suggesting significant electronic interactions within the newly assembled CD@AgNPs. This appears clearly from the comparisons proposed in Figure S5(a) and Figure S5(b) where the experimentally acquired extinction spectra (orange curves) of CD@AgNP- and CD@AgNP+ are directly overlayed to the extinction spectra theoretically expected in the trivial case of no interaction (green dashed curves), which are simply obtained by a simple appropriate linear combination of the experimental spectra of the two isolated components. Such differences indicate the existence of a strong interaction between CDs and AgNP already at the ground state level, that is, the formation of stable CD@AgNP complexes. Also in this case, the effect is more evident in the case of AgNP+, consistent with the photoluminescence data in Figure 2(a) and (b).

Finally, nanosecond time-resolved fluorescence measurements fully confirm these interpretations. In fact, we observe for both CD@AgNP- and CD@AgNP+ the same fluorescence decay kinetics observed in naked CDs, except for a lower initial intensity (panel (d) of Fig 2). The naked CDs emission decay can be described as a stretched exponential decay with a lifetime of $\tau = 4.7 \pm 0.2$ ns and a stretching parameter of $\beta = 0.84 \pm 0.02$. The emission lifetimes obtained in the case of CD@AgNP- and CD@AgNP+ solutions are identical (see Fig. 2d), which clearly rules out the possibility of a collisional photoluminescence quenching mechanism, which would cause a decrease of the PL lifetimes proportional to the quencher concentration. Indeed, a diffusional-type quenching would be extremely unlikely considering the very low concentration of silver nanoparticles involved. In contrast, an intensity decrease with no changes in lifetime, such as observed in Fig. 2d, is typical of static quenching produced within stable complexes held together by ground-state interactions [43].

In addition to the spectroscopic characterization, the CD@AgNP+ solutions were analyzed also by HRTEM (Figure S6). Because of the low electron density of CDs, it is generally very difficult to directly image CDs when they are close to AgNPs surfaces. Despite that, we were able to find by HRTEM at least a few examples of CDs clearly adhering to the surface of silver nanoparticles, further corroborating that quenching occurs through the formation of stable CD@AgNP nanohybrids upon self-assembly of the two components in solution phase.

Thus, all the data hitherto reported clearly show that CDs are able to spontaneously bind to both AgNP- and AgNP+ in solution phase. At the same time, the absence of changes in the nanosecond lifetime implies that the dynamical pathways provoking the emission quenching in photoexcited CD@AgNP hybrids must entirely occur on a sub-nanosecond time-scale.

Previous computational and experimental studies of CDs have suggested that their photo-excited state features an excess of negative charge on surface groups [37, 44], making CDs very good photoexcited electron donors. In CD@AgNP+ we expect that the transfer of a photoexcited electron to positively-charged metal nanoparticles should be energetically downhill, also considering that the Fermi level of silver (reported at -4.7 eV for bulk Ag *vs* vacuum energy level [45]) is located at lower energies than the LUMO of CDs (around -4.0 eV *vs* vacuum energy level [46]). Therefore, the quenching observed in CD@AgNP+ is most likely attributed to an electron transfer from CDs to AgNPs, as often observed for chromophores in the vicinity of metal surfaces [47]. Such a behavior may then results in the formation of a photocatalytically-active charge-separated pair across the CD-AgNP interface, interesting for applications. In regard to CD@AgNP- one may expect the electron transfer to be less efficient or entirely blocked by the negative excess charge on the acceptor. The fundamental mechanisms may thus be different in the two cases, as further investigated in the following.

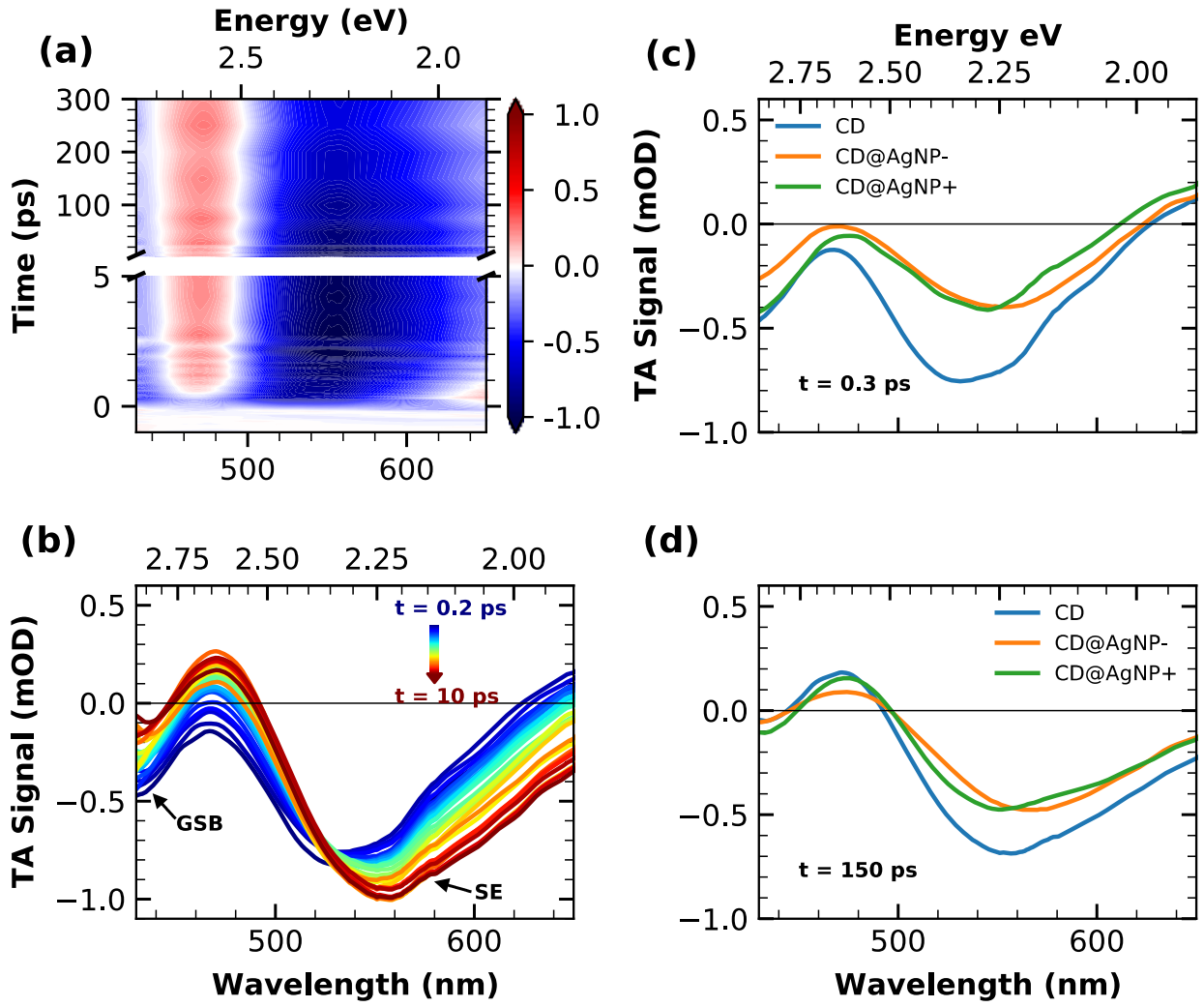


*Figure 3 – (a) Time-wavelength TA plot of bare CD aqueous solution upon 400 nm excitation and at magic angle detection. (b) Selected TA spectra at different delays from photoexcitation, continuously increasing from 0.2 ps (blue line) to 10 ps (red line), as obtained by horizontal cuts of 2D-plot of panel (a). Comparison of TA spectra of bare CDs (blue), CD@AgNP- (orange) and CD@AgNP+ (green) solutions recorded at (c) 0.3 ps and (d) 150 ps after photoexcitation.*

On this basis we carried out femtosecond transient absorption (TA) measurements exciting with 150 fs duration pulses at 400 nm, with the aim of comparing the relaxation dynamics of the naked CDs with that of the two nanohybrids CD@AgNP- and CD@AgNP+.

In Figure 3a, the TA data collected from the solution of bare CDs are reported as a time-wavelength 2D plot, from which we extracted the spectra at different delays from photoexcitation shown in panel b. It is possible to identify two main components in the TA signal: (i) a negative contribution in the proximity of the pump wavelength (400 nm), mostly associated to ground state bleaching (GSB) due to the ground-state depopulation caused by pump absorption, (ii) a strong stimulated emission (SE), which is equivalent to an ordinary fluorescence signal (except for its negative sign), and is observed to shift from 520 to 550 nm with time. The main spectral evolution observed consists of a dynamical

Stokes shift of the fluorescence (that is, the SE), taking place in the very first picoseconds, attributed to a solvatochromic relaxation [37]. In Figure 3b, we also see a reduction of the negative signal close to the pump wavelength. This is due to the partial disappearance of an overlapping blue SE signal, which will not be further discussed here [37].

The same experiment was carried out for solution of CD@AgNP- and CD@AgNP+ nanohybrids, prepared in such a way that the CDs concentration was the same to that of bare CDs. When the experiment is carried out in identical conditions, the TA signals observed in the nanohybrids are overall similar to bare CDs, but the comparisons displayed on the right side of Figure 3 show several important differences. In fact, the negative component associated to SE appears to be clearly less intense in the case of CD@AgNP nanohybrids at all delays, as shown in panel (c) for the earliest spectrum at 300 fs. Being the SE equivalent to fluorescence, this represents an additional evidence of the quenching of CDs emission by both types of AgNPs. Most importantly, it reveals that quenching is very fast and takes place within 300 fs from photo-excitation.

Comparing the GSB signals gives additional information on the mechanism responsible for the quenching. For the complexes formed with positively-charged AgNPs, we observe a perfect match between the GSB signals of CD and CD@AgNP+, despite the reduction in the SE, indicating that CDs have not returned to their ground state after quenching. Such a result is fully in line to the hypothesis of an electron transfer between CDs and AgNP+, occurring in less than 300 fs. In fact, the transfer of a photo-excited electron from CDs to interacting AgNP+ is expected to leave an unpaired hole in CDs, so preventing their return to their ground state. Interestingly, the GSB signals in bare CDs and CD@AgNP+ become very similar to each other at long times (Figure 3d, 150 ps), as better highlighted from the normalized comparison proposed in Figure S7, suggesting that the charge-separated state eventually recombines through back electron transfer (BET) from AgNPs to CDs.

In regard to CD@AgNP-, we would expect an electron transfer to be hindered by the negative surface charge of the acceptor metal nanoparticle. In fact, the data collected on CD@AgNP- at early times (Figure 3c) show that in this case the fluorescence quenching (reduction of the SE) is accompanied the return of CDs to their ground state, as inferred from the corresponding weakening of the GSB signal (compare blue and orange curves at 420 nm). This difference can be explained if we assume that, instead of electron transfer, CD@AgNP- undergo an energy transfer from the excited CDs to the nearby MNP, that is, the whole electron-hole pair initially formed on CDs is transferred to AgNPs, leading to the concurrent quenching of both the SE and the GSB signal of CDs. Another explanation would be assuming the occurrence for the CD@AgNP- of a very fast BET. In practice, an energy transfer cannot be distinguished from a rapid sequence of electron and back-electron transfer, considering that both these processes all occur within our time resolution.

To quantify the times scales and the associated spectral evolution, we decompose the experimental data of the three experiments *via* singular value decomposition (SVD) global analysis [34]. The results of this analysis are shown in Figure S8 (DAS spectra and associated lifetimes) and Figure S9 (fitting curves of selected time traces). In accordance with the aforementioned explanation, the entire spectral evolutions of CD and CD@AgNP- samples are essentially fully described by similar decay associated spectra (DAS) only differing by a constant factor, associated to the same lifetimes $\tau_1 = 0.9 \pm 0.2$ ps and $\tau_2 > 500$ ps (Figure S8(a) and (b)). The process with time constant $\tau_2$ refers to the slow depopulation of the excited state at long times, and the parallel recovery of the ground state; the time scale $\tau_1$ accounts for the red-shift of the spectrum due to solvation dynamics, as confirmed by the derivative-like line shape with a zero close to the SE peak. Considering that in this case the photoexcited CDs undergo an energy transfer to the AgNPs, the measured TA signal for CD@AgNP- solution entirely originates from the fraction of CDs in solution not bound to AgNP-. Therefore, the TA dynamics observed in CD@AgNP- and bare CDs should be almost identical, as observed.

On the contrary, as shown in Figure S8(c), an additional dynamical component was found in the case of CD@AgNP+ solution, associated to a lifetime of $\tau = 11 \pm 2$ ps. Considering that this process occurs much later than the quasi-instantaneous (<300 fs) electron transfer, we attribute it to a BET from AgNP+ to the CD, ultimately closing the photocycle of the complex. Overall, our TA data confirm the ultrafast formation of a relatively long-lived (11 ps) photoinduced charge separated state in CD@AgNP+ complexes. In contrast, CD@AgNP- nanohybrids appear incapable of hosting a long-lived charge-separated pair. Their photocycle either proceeds through energy transfer from CDs to the nearby metal, or by a fast sequence of forward and back-electron transfer, completed within hundreds of femtoseconds from photoexcitation.

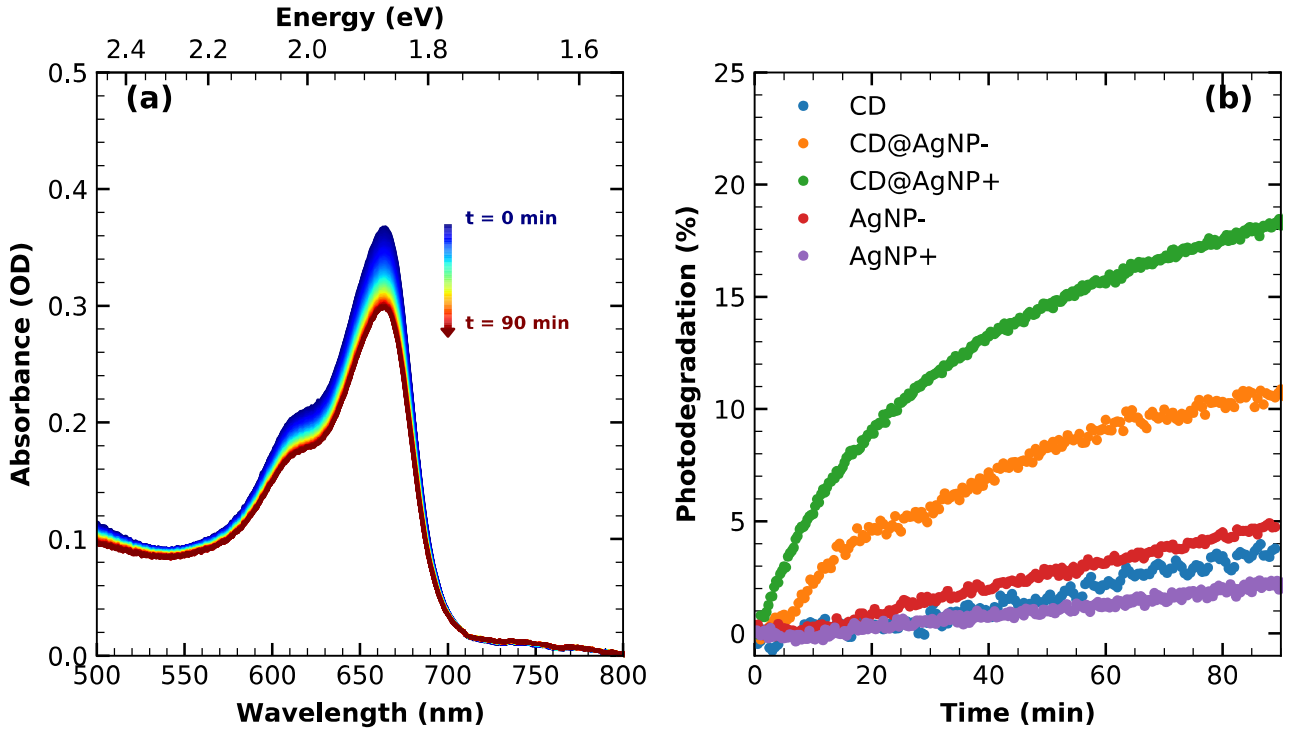


*Figure 4 – (a) UV-vis absorbance spectra of methylene blue as a function of time under continuous illumination in presence of CD@AgNP+. (b) Percentage of methylene blue photodegradation under continuous illumination in the presence of bare CD (blue), CD@AgNP- (orange), CD@AgNP+ (green), pure AgNP+ (red) and pure AgNP+ (violet).*

On these grounds, we decided to test the photocatalytic activities of the two nanohybrids by evaluating the photodegradation of methylene blue (MB) under VIS-UV light irradiation.

The MB photodegradation treatments were carried out by using either the nanohybrids CD@AgNP- and CD@AgNP+ as photocatalysts, and three additional reference experiments were conducted employing pure CD, and bare AgNP- and AgNP+ solutions respectively. In order to make the comparison homogeneous, the experiments were conducted on five equally concentrated solutions of methylene blue to which comparable quantities of photocatalysts were added each time.

The MB photodegradation was evaluated via a continuous acquisition of its absorbance spectrum over 90 minutes under illumination by a Xe lamp (see experimental section). The results are displayed in left panel of Figure 4, where the absorbance spectra of MB/CD@AgNP+ are overlayed using a color scale accounting for different time delays from the starting of light irradiation. The right panel of the same Figure shows the percentage of MB removal *vs* time for the five samples, directly estimated by the absorbance. Very little photodegradation of MB was found in the three control experiments, although pure AgNP- and AgNP+ showed respectively a slightly higher and lower photocatalytic efficiency than that of CD, probably associated to a different percentage of MB adsorption over the photocatalysts due to the cationic nature of the dye. In contrast, the two nanohybrids revealed a much stronger photodegradation activity: within 90 minutes of light exposure,

the CD@AgNP- photocatalyst was able to reduce more than 10 % of MB content while an almost double value was achieved with CD@AgNP+. This result is again consistent with the observations of stronger electronic interactions in the latter (Figure 2), especially when considering that the photodegradation efficiency for CD@AgNP+ is probably reduced by the cationic nature of MB while, on the contrary, it is favored in the case of CD@AgNP- nanohybrids, which are expected to provide a much larger active surface to the local attachment of MB.

The result of these experiments, although at a proof-of-concept level, provide further indications of the undergoing processes, confirming the initial hypotheses motivating this study. Indeed, both types of CD@AgNP nanohybrids are characterized by a significant emergent photocatalytic activity not found in either of the two starting precursors. The enhanced photocatalytic activity of CD@AgNP+ nanohybrids can be well understood on the basis of the facilitated electron-transfer mechanism between CD and AgNP+. Photoexcited electron transfer from CDs produces quasi-free electrons on AgNP available for further reactions, ultimately responsible of degrading the MB dye. In regard to CD@AgNP- nanohybrids, we have argued before that their interaction can be described either as an energy transfer or as fast sequence of forward and back-electron transfer, which cannot be distinguished within our experimental time resolution. In this respect, the observation of MB photodegradation also in the case of CD@AgNP- nanohybrids would seem to suggest the latter interpretation. Moreover, in this case the coexistence of an additional photodegradation mechanism of methylene blue involving hydroxy radicals produced by photoholes [48] cannot be completely ruled out, which could also account for the ultrafast CD ground state recovery highlighted by TA data. Nevertheless, further femtosecond TA studies with higher time resolution will be needed to fully address this aspect.

# Conclusions

We reported an easy route to synthesize CD-AgNP nanohybrids from the spontaneous self-assembly of the two nanomaterials in solution phase. On the basis of a fully detailed optical investigation from steady state to the femtosecond range, we had evidence of the successful coupling between the CDs and AgNPs, mainly highlighted by a static quenching of CDs emission due to a very efficient photoinduced electron transfer happening within 300 fs, and followed by a comparatively slow (11 ps) back electron transfer. Photocatalytic proof-of-concept tests demonstrate that CD@AgNP nanohybrids display a significant emergent photocatalytic activity that is absent in the starting component and can be attributed to the electronic interactions within the systems. Moreover,

we demonstrate that controlling surface charges is crucial in the design of functional CD@AgNP nanohybrids. Although CDs can be successfully coupled to negatively-charged AgNPs-, the negative charge on the metal nanoparticles reduces the fraction of CDs which successfully bind to them, hinders electron transfer and the consequent formation of a long-lived charge separated pair which is eventually responsible of photocatalytic response. Beside contributing to clarify the specific interactions between CDs and silver nanoparticles at a fundamental level, our results are very promising in view of the development of a new class of eco-friendly functional nanohybrids for light-driven catalytic applications.

# References


[1] Y.-P. Sun, B. Zhou, Y. Lin, W. Wang, K. A. S. Fernando, P. Pathak, M. J. Meziani, B. A. Harruff, X. Wang, H. Wang, P. G. Luo, H. Yang, M. E. Kose and B. Chen, *J. Am. Chem. Soc.,* 2006, **128**, 7756.

[2] J. Liu, R. Li and B. Yang, *ACS Cent. Sci.,* 2020, **6**, 2179.

[3] A. Cayuela, M. L. Soriano and M. Valcárcel, *Analytica Chimica Acta,* 2013, **804**, 246.

[4] G. Ragazzon, A. Cadranel, E. V. Ushakova, Y. Wang, D. M. Guldi, A. L. Rogach, N. A. Kotov and M. Prato, *Chem.,* 2021, **7**, 606.

[5] J. B. Essner and G. A. Baker, *Environ. Sci.: Nano,* 2017, **4**, 1216.

[6] Q.-L. Chen, C.-F. Wang and S. Chen, *Journal of Materials Science,* 2013, **48**, 2352.

[7] X. Yang, Y. Zhuo, S. Zhu, Y. Luo, Y. Feng and Y. Dou, *Biosensors & bioelectronics,* 2014, **60**, 292.

[8] H. Zhang, Y. Chen, M. Liang, L. Xu, S. Qi, H. Chen and X. Chen, *Anal. Chem.,* 2014, **86**, 9846.

[9] J. Pardo, Z. Peng and R. M. Leblanc, *Molecules,* 2018, **23**, 378.

[10] M. Zheng, S. Ruan, S. Liu, T. Sun, D. Qu, H. Zhao, Z. Xie, H. Gao, X. Jing and Z. Sun, *ACS Nano,* 2015, **9**, 11455.

[11] N. Aich, J. Plazas-Tuttle, J. Lead and N. Saleh, *Environmental Chemistry ,* 2014, **11**, 609.

[12] N. C. Bigall, W. J. Parak and D. Dorfs, *Nano Today,* 2012, **7**, 282.

[13] Y. Liu, S. Roy, S. Sarkar, Y. Zhao and J. Zhang, *Carbon Energy,* 2021, **3**, 795.

[14] A. Madonia, M. Martin-Sabi, A. Sciortino, S. Agnello, M. Cannas, S. Ammar, F. Messina and D. Schaming, *J. Phys. Chem. Lett.,* 2020, **11**, 4379.

[15] A. Cadranel, J. T. Margraf, V. Strauss, T. Clark and D. Guldi, *Acc. Chem. Res.*, 2019, **52**, 955.

[16] M. Zulfajri, S. Sudewi, S. Ismulyati, A. Rasool, M. Adlim and G. G. Huang, *Coatings,* 2021, **11**, 1100.

[17] Z. Ma, H. Ming, H. Huang, Y. Liu and Z. Kang, *New J. Chem.,* 2012, **36**, 861.

[18] S. Bhattacharyya, F. Ehrat, P. Urban, R. Teves, R. Wyrwich, M. Döblinger, J. Feldmann, A. S. Urban and J. K. Stolarczyk, *Nature Communications,* 2017, **8**, 1401.

[19] S. Chandra, S. Pradhan, S. Mitra, P. Patra, A. Bhattacharya, P. Pramanikb and A. Goswamia, *Nanoscale,* 2014, **6**, 3647.

[20] S. Xie, H. Su, W. Wei, M. Li, Y. Tong and Z. Mao, *J. Mater. Chem. A,* 2014, **2**, 16365.

[21] L. Cao, S. Sahu, P. Anilkumar, C. E. Bunker, J. Xu, K. A. S. Fernando, P. Wang, E. A. Guliants, K. N. Tackett and Y.-P. Sun, *J. Am. Chem. Soc.,* 2011, **133**, 4754.

[22] X. Yan, X. Cui, B. Li and L.-s. Li, *Nano Lett.,* 2010, **10**, 1869.

[23] H. Ming, Z. Ma, Y. Liu, K. Pan, H. Yu, F. Wang and Z. Kang, *Dalton Trans.,* 2012, **41**, 9526.

[24] X. Yu, J. Liu, Y. Yingchun, S. Zuo and B. Li, *Carbon,* 2014, **68**, 718.

[25] H. Li, R. Liu, Y. Liu, H. Huang, H. Yu, H. Ming, S. Lian and S.-T. a. Z. Kang, *J. Mater. Chem*, 2012, **22***, 17470*.

[26] A. N. Emam, S. A. Loutfy, A. A. Mostafa, H. Awad and M. B. Mohamed, *RSC Adv.,* 2017, **7**, 23502.

[27] K. Yuan, R. Qin, J. Yu, X. Li, L. Li, X. Yang, X. Yu, Z. Lu, X. Zhang and H. Liu, *Applied Surface Science,* 2020, **502**, 144277.

[28] Y. Liu, C. Liu, Z. Zhang, W. Yang and S. Nie, *J. Mater. Chem. C,* 2015, **3**, 2881.

[29] R. Liu, H. Li, W. Kong, J. Liu, Y. Liu, C. Tong, X. Zhang and Z. Kang, *Materials Research Bulletin,* 2013, **48**, 2529.

[30] F. Messina, L. Sciortino, R. Popescu, A. M. Venezia, A. Sciortino, G. Buscarino, S. Agnello, R. Schneider, D. Gerthsen, M. Cannas, F. M. Gelardi, *J. Mater. Chem. C*, 2016, **4**, 2598.

[31] A. Sciortino, N. Mauro, G. Buscarino, L. Sciortino, R. Popescu, R. Schneider, G. Giammona, D. Gerthsen, M. Cannas and F. Messina, *Chem. Mater.,* 2018, **30**, 1695.

[32] J. Turkevich, P. C. Stevenson and J. Hillier, *Discuss. Faraday Soc.,* 1951, **11**, 55.

[33] D. Paramelle, A. Sadovoy, S. Gorelik, P. Free, J. Hobley and D. G. Fernig, *Analyst,* 2014, **139**, 4855.

[34] C. Ruckebusch, M. Sliwa, P. Pernot, A. de Juan and R. Tauler, *Journal of Photochemistry and Photobiology C: Photochemistry Reviews,* 2012, **13**, 1.

[35] Y. H. Yuan, Z. X. Liu, R. S. Li, H. Y. Zou, M. Lin, H. Liu and C. Z. Huang, *Nanoscale,* 2016, **8**, 6770.

[36] J. Zhou, Y. Yang and C. Zhang, *Chem. Commun.,* 2013, **49**, 8605.

[37] M. Gazzetto, A. Sciortino, M. Nazari, E. Rohwer, G. Giammona, N. Mauro, T. Feurer, F. Messina and A. Cannizzo, *ACS Appl. Nano Mater.,* 2020, **3**, 6925.

[38] R. C. Fernández-Hernández, R. Gleason-Villagran, C. Torres-Torres, L. Rodríguez-Fernández, A. Crespo-Sosa, J. C. Cheang-Wong, A. López-Suárez, R. Rangel-Rojo, A. Oliver and J. A. Reyes-Esqueda, *J. Opt.,* 2012, **14**, 125203.

[39] D. Wang, N. B. Saleh, W. Sun, C. M. Park, C. Shen, N. Aich, W. J. G. M. Peijnenburg, W. Zhang, Y. Jin and C. Su, *Environ. Sci. Technol.,* 2019, **53**, 7265.

[40] S. Skoglund, E. Blomberg, I. O. Wallinder, I. Grillo, J. S. Pedersen and L. M. Bergström, *Phys. Chem. Chem. Phys.,* 2017, **19**, 28037.

[41] J. Lim, N.-E. Lee, E. Lee and S. Yoon, *Bull. Korean Chem. Soc.,* 2014, **35**, 2567.

[42] U. Kreibig and M. Vollmer, *Berlin: Springer*, 1995.

[43] A. Sciortino, A. Madonia, M. Gazzetto, L. Sciortino, E. J. Rohwer, T. Feurer, F. M. Gelardi, M. Cannas, A. Cannizzo and F. Messina, *Nanoscale,* 2017, **9**, 11902.

[44] A. Sciortino, F. Ferrante, N. Mauro, G. Buscarino, L. Sciortino, G. Giammona, M. Cannas, D. Duca and F. Messina, *Carbon,* 2021, **173**, 454.

[45] X. Zhang, Y. L. Chen, R.-S. Liu and D. P. Tsai, *Rep. Prog. Phys.,* 2013, **76**, 1.

[46] A. Armano, G. Buscarino, F. Messina, A. Sciortino, M. Cannas, F. M. Gelardi, F. Giannazzo, E. Schilirò and S. Agnello, *Nanomaterials,* 2020, **10**, 528.

[47] P. V. Kamat, J. *Phys. Chem. B ,* 2002, **106**, 7729.

[48] A. Houas, H. Lachheb, M. Ksibi, E. Elaloui, C. Guillard, J.-M. Herrmann, *Applied Catalysis B: Environmental*, 2001, **31**, 145.